PERGAMON

Progress in Biophysics & Molecular Biology 69 (1998) 157–183

Progress in Biophysics & Molecular Biology

Three-dimensional analysis of regional cardiac function: a model of rabbit ventricular anatomy

Frederick J. Vetter, Andrew D. McCulloch *

Department of Bioengineering, University of California San Diego, 9500 Gilman Drive, La Jolla, CA 92093-0412, USA

Abstract

The three-dimensional geometry and anisotropic properties of the heart give rise to nonhomogeneous distributions of stress, strain, electrical activation and repolarization. In this article we review the ventricular geometry and myofiber architecture of the heart, and the experimental and modeling studies of three-dimensional cardiac mechanics and electrophysiology. The development of a three-dimensional finite element model of the rabbit ventricular geometry and fiber architecture is described in detail. Finally, we review the experimental results, from the level of the cell to the intact organ, which motivate the development of coupled three-dimensional models of cardiac electromechanics and mechanoelectric feedback.

1. The need for three-dimensional models

The dynamic pumping function of the heart depends on cellular ionic mechanisms which give rise to the cardiac action potential, the crossbridge interactions that develop myofilament tension, and intracellular calcium fluxes that regulate contraction. To understand how these processes govern the mechanics and electrophysiology of the intact myocardium requires knowledge of the three-dimensional geometry and structure of the whole heart. Normal myocardium is heterogeneous (Brutsaert, 1987). The normal heart exhibits nonhomogeneous distributions of stress, strain, electrical activation and repolarization (Durrer et al., 1970; Waldman et al., 1988; Efimov et al., 1996). These heterogeneities are frequently exaggerated in pathological conditions such as myocardial ischemia (Lew, 1987; Villarreal et al., 1991; Kurz et al., 1994; Van Leuven et al., 1994). Three-dimensional models provide a way to investigate how regional mechanics and electrical propagation depend on local properties.

Although many important variables can be experimentally measured in cardiac cells or in the whole heart, practical methods for measuring their three-dimensional variations throughout the

* Corresponding author. Fax: +1-619-534-6896; E-mail: amcculloch@ucsd.edu

0079-6107/98/$19.00
PII: S0079-6107(98)00006-6

myocardium are highly limited. Hence there is a need for three-dimensional models of myocardial electrical and mechanical function based on the underlying biophysics of the cell and a realistic representation of regional ventricular geometry and fiber architecture.

In a review article published in this journal, Hunter and Smaill (1988) outlined how a continuum approach could be used to achieve these goals in practice. Continuum models must be represented in a manner suitable for efficient and accurate computation. The finite element method is capable of formulating and solving nonlinear continuum problems on irregular and anisotropic physical structures and thus provides a framework for the development and use of practical continuum models. In this report we set out to: (1) review the three-dimensional ventricular geometry and fiber architecture of the mammalian heart, (2) discuss experimental observations and models of cardiac mechanics and electrophysiology, (3) present a new model of the rabbit heart ventricular anatomy and (4) discuss future applications.

2. Structure

2.1. Ventricular geometry

From the perspective of engineering mechanics, the ventricles are three-dimensional thick-walled pressure vessels with substantial variations in wall thickness and principal curvatures both regionally and temporally through the cardiac cycle. The ventricular walls in the normal heart are thickest at the equator and base of the left ventricle and thinnest at the left ventricular apex and right ventricular free wall. There are also variations in the principal dimensions of the left ventricle with species, age, phase of the cardiac cycle, and disease. In general, however, the ratio of wall thickness to radius is too high to be treated accurately by all but the most sophisticated thick-wall shell theories (Taber, 1991).

Ventricular geometry has been studied in most quantitative detail in the dog heart (Streeter and Hanna, 1973a; Nielsen et al., 1991). Geometric models have been very useful in the analysis, especially the use of confocal and nonconfocal ellipses of revolution to describe the epicardial and endocardial surfaces of the left and right ventricular walls. The canine left ventricle is reasonably modeled by a thick ellipsoid of revolution truncated at the base. The crescentic right ventricle wraps about 180° around the heart wall circumferentially and extends longitudinally roughly two-thirds of the distance from the base to the apex. Using a truncated ellipsoidal model, left ventricular geometry in the dog can be defined by the major and minor radii of two surfaces, the left ventricular endocardium and a surface defining the free wall epicardium and the septal endocardium of the right ventricle. Streeter and Hanna (1973a) described the position of the basal plane using a truncation factor f_b defined as the ratio between the longitudinal distances from equator-to-base and equator-to-apex. Hence, the overall longitudinal distance from base to apex is $(1 + f_b)$ times the major radius of the ellipse. Since variations in f_b between diastole and systole are relatively small (0.45 to 0.51), they suggested a constant value of 0.5.

The focal length d of an ellipsoid is defined from the major and minor radii (a and b) by $d^2 = a^2 - b^2$ and varies only slightly in the dog from endocardium to epicardium between end-diastole (37.3 to 37.9 mm) and end-systole (37.7 to 37.1 mm) (Streeter and Hanna, 1973a).

Hence, within the accuracy that the boundaries of left ventricular wall can be treated as ellipsoids of revolution, the assumption that the ellipsoids are confocal appears to be a good one. This has motivated the choice of prolate spheroidal (elliptic-hyperbolic-polar) coordinates (λ, μ, θ) as a system for economically representing ventricular geometries obtained post-mortem or by noninvasive tomography (Nielsen et al., 1991; Young and Axel, 1992). The Cartesian coordinates of a point are given in terms of its prolate spheroidal coordinates (see Fig. 4b) by

$$x_1 = d\cosh\lambda\cos\mu, \qquad x_2 = d\sinh\lambda\sin\mu\cos\theta, \qquad x_3 = d\sinh\lambda\sin\mu\sin\theta \tag{1}$$

Here, the focal length d defines a family of coordinate systems that vary from spherical polar when $d = 0$ to cylindrical polar in the limit as $d \to \infty$. A surface of constant transmural coordinate λ is an ellipse of revolution with major radius $a = d\cosh\lambda$ and minor radius $b = d\sinh\lambda$.

2.2. Myofiber architecture

The cardiac ventricles have a complex three-dimensional muscle fiber architecture (for a comprehensive review see Streeter et al. (1978)). Although the myocytes are relatively short, they are connected such that at any point in the normal heart wall there is a clear predominant fiber axis that is approximately tangent with the wall (within 3–5° in most regions, except near the apex and papillary muscle insertions). Each ventricular myocyte is connected via gap junctions at intercalated disks to an average of 11.3 ± 2.2 neighbors (Saffitz et al., 1994). From the sixteenth century studies of Vesalius up to 1942 (Robb and Robb, 1942), investigators dissected discrete bundles of fibrous swirls (Greenbaum et al. (1981) provide a historical synopsis), but more modern histological techniques have shown that in the plane of the wall, the muscle fiber angle makes a smooth transmural transition from epicardium to endocardium. Similar patterns have been described for humans (Pearlman et al., 1982), dogs (Streeter et al., 1969), macaques (Ross and Streeter, 1975), pigs (Streeter and Bassett, 1966), guinea pigs (Hort, 1960) and rats (Omens et al., 1993). In the human or dog left ventricle, the muscle fiber angle typically varies continuously from about −60° (i.e. 60° clockwise from the circumferential axis) at the epicardium to about +70° at the endocardium. The rate of change of fiber angle is usually greatest at the epicardium, so that circumferential (0°) fibers are found in the outer half of the wall and begins to slow approaching the inner third near the trabeculata–compacta interface.

Regional variations in ventricular myofiber orientations are generally smooth except at the junction between the right ventricular free wall and septum. A detailed study in the dog that mapped fiber angles throughout the entire right and left ventricles described the same general transmural pattern in all regions including the septum and right ventricular free wall, but with definite regional variations (Nielsen et al., 1991). Transmural differences in fiber angle were about 120–140° in the left ventricular free wall, larger in the septum (160–180°) and smaller in the right ventricular free wall (100–120°). There are also small increases in fiber orientation from end-diastole to systole (7–19°), with greatest changes at the epicardium and apex (Streeter et al., 1969).

Collagen is the major structural protein in connective tissues but only comprises 2–5% of the myocardium by weight, compared with the myocytes which make up 90% (Weber, 1989). The collagen matrix has a hierarchical organization and has been classified according to conventions established for skeletal muscle into endomysium, perimysium, and epimysium (Caulfield and Borg, 1979; Robinson et al., 1983). The endomysium is associated with individual cells and includes a fine weave surrounding the cell and transverse structural connections connecting adjacent myocytes, with attachments localized near the z-line of the sarcomere. The perimysium groups cells together and includes large coiled fibers typically 1–3 microns in diameter composed of smaller collagen fibrils (40–50 nm) (Robinson et al., 1988) as well as the collagen fibers that wrap bundles of cells forming laminar sheets 3–4 cells thick which radially traverse the ventricular wall (LeGrice et al., 1995). Finally, a thick epimysial collagen sheath surrounds the entire myocardium forming the protective epicardium (visceral pericardium) and endocardium.

3. Three-dimensional mechanics

3.1. Experimental investigations

The distribution of wall stress in the myocardium is fundamentally important because it affects ventricular pumping performance, myocardial oxygen demand, coronary blood flow, vulnerability to injury, myocyte growth and remodeling and action potential shape and propagation (McCulloch and Omens, 1991; McCulloch, 1995). No successful methods have been developed to measure the three-dimensional stress tensor in the intact heart wall primarily because of its large deformations and the tissue injury caused by implanted transducers (Huisman et al., 1980). However, methods have been developed to measure regional distributions of two- and three-dimensional deformations in the resting and beating canine, rat and mouse heart using ultrasonic crystals (Villarreal et al., 1988; Omens et al., 1996) and biplane video imaging or radiography of closely spaced material markers (Waldman et al., 1985; Waldman et al., 1988; McCulloch et al., 1989; Omens et al., 1991). MRI tagging methods have been used to measure three-dimensional ventricular strain distributions non-invasively (Moore et al., 1992; Young and Axel, 1992; Azhari et al., 1993). These experiments have shown substantial regional and transmural strain heterogeneity even in the healthy heart and provide data to validate models of ventricular mechanics.

The distributions of stress in the heart are governed by the three-dimensional structure of the ventricular walls, the material properties of the myofibers and the collagen matrix in the relaxed and actively contracting states and the boundary conditions imposed by cavity pressures and structures such as the valve annulus, chordae tendineae, pericardium and lungs. Many of these factors have been measured in the laboratory, including geometry and myocardial fiber architecture (Streeter and Hanna, 1973a,b; Nielsen et al., 1991), laminar myofiber sheet orientations (LeGrice et al., 1995) and passive and active uniaxial mechanical properties of isolated cardiac muscle (Pinto and Fung, 1973; ter Keurs et al., 1980). Although fully triaxial material testing still presents significant difficulties, biaxial

stress–strain testing has been performed in freshly excised specimens of canine myocardium (Yin et al., 1987; Novak et al., 1994), epicardium (Humphrey and Yin, 1988) and pericardium (Lee et al., 1987).

3.2. Mechanics modeling

Models are needed to understand cardiac mechanics in terms of regional stress and strain distributions. An accurate model should include the three-dimensional ventricular geometry, fiber and connective tissue architecture, the nonlinear, history-dependent constitutive properties of the myocardium during systole and diastole and the pressure and displacement boundary conditions. Other important factors include the effects of blood perfusion and residual stress (McCulloch et al., 1993; Guccione et al., 1995; Costa et al., 1996a).

Many workers have used the finite element (FE) method as a parametric framework for analysis of regional function in the heart as a three-dimensional continuum (Province et al., 1993; Bovendeerd et al., 1994; Young et al., 1994). The FE method provides an efficient and accurate means to both develop detailed anatomical continuum models and conduct numerical analyses of biological phenomena. High-order FE models are typically very compact — they can represent a large number of physical parameters using relatively few model variables ('degrees of freedom' or DOF). Two significant capabilities of the FE method when applied to cardiac modeling are the ability to represent and analyze irregularly shaped physical domains that may undergo large deformations and the provision for nonuniform domain discretization.

An accurate and mathematically compact structural model of the ventricular geometry and fiber architecture is prerequisite for simulating the effect of heterogeneous three-dimensional mechanics on the electrical behavior of intact myocardium. Nielsen et al. (1991) developed the first fully three-dimensional FE model of the canine ventricular geometry and nonuniform fiber distribution. Their model clearly demonstrates the compactness of the FE formulation by representing over 1,300 measured geometric coordinates with 240 DOF and 8,690 fiber orientation measurements with 396 DOF. This model provided the foundation for the practical solution of large-scale cardiac stress analyses. The model was recently extended to include the laminar sheet structure of myocardium (LeGrice et al., 1997), a feature that will be useful in the study of microstructural influences on mechanical deformation and electrical propagation in myocardium.

Costa et al. (1996a) have developed and rigorously validated novel nonlinear FE methods for the three-dimensional analysis of ventricular wall stress. The Galerkin FE formulation includes important characteristics of ventricular mechanics such large deformations, nonlinear elasticity, curvilinear coordinates, three-dimensional anisotropy with respect to continuously varying myofiber axes, muscle contraction and pressure and displacement boundary conditions (Guccione et al., 1995). Stress and strain solutions that are converged to within 0.2% can be obtained for a model of the diastolic left ventricle with 16–32 tricubic Hermite elements and computations can be completed in 1–2 h on a Silicon Graphics R4400 workstation (Costa et al., 1996b).

Comparing the results of transversely isotropic models (Guccione et al., 1991) with three-dimensional strains measured in the isolated and intact dog heart (Waldman et al., 1985;

Omens et al., 1991) has shown that these models generally agree very well with the observed strains. The biggest single shortcoming of the present models is that whereas they fairly well approximate regional diastolic strains and most components of the strain during systole, they do not accurately predict the transmural distributions of transverse shear strain components measured during systole (Waldman et al., 1985, 1988; Omens and Covell, 1991). The only other models to include complete results on three-dimensional strains (Bovendeerd et al., 1992) have also demonstrated this limitation. Costa provided theoretical and experimental evidence that incorporating the effects of myocardial cleavage planes with transversely oriented layers of muscle fibers about 4 cells thick (Smaill and Hunter, 1991; LeGrice et al., 1995) in the models, with an appropriate choice of orthotropic material parameters, may overcome this limitation (Costa, 1996). Among other findings, these models have shown that there is substantial regional heterogeneity of ventricular mechanics even under normal conditions (Costa et al., 1996b), with the notable exception of the fiber strain distribution which is comparatively uniform despite significant variations in fiber stress and the strains in other directions. One mechanism of this fiber strain uniformity is the torsional deformation that results from the helical fiber orientations and the anisotropy of the resting and active myocardium (Guccione et al., 1991).

4. Three-dimensional electrophysiology

4.1. Experimental investigations

The time–course of the cardiac action potential is governed by ionic currents via transmembrane channels, pumps and exchangers which determine the excitability and refractoriness of the tissue. Electrical excitation in the ventricles is nonuniform (Durrer et al., 1970). Facilitated by the His-Purkinje system, endocardial excitation propagates radially to the epicardium, though the apical and central regions are activated earlier than the base. With respect to the myofibers, propagation is generally 2–4 times faster in the longitudinal than transverse direction (Delgado et al., 1990; Knisley and Hill, 1995). Developing an understanding of cardiac activation and recovery patterns has been difficult because of the geometric and structural complexity of the heart and the fine spatial scale of the activation patterns relative to the whole organ. At the scale of the laminar sheets, LeGrice et al. (1995) propose that the intrinsic conduction velocity transverse to the myofiber is 2–3 times greater in the plane of the sheet than perpendicular to it. Experimental confirmation of this hypothesis is lacking, however, due to the inherent difficulty of measuring conduction patterns and activation times in three-dimensional tissue preparations. Wavefront geometry also plays a role in the speed of the propagating wave, increasing the velocity when the wavefront is curved toward the direction of propagation. When the wavefront curved away from the direction of propagation, the velocity decreases and may vanish above a critical radius of curvature (Cabo et al., 1994, 1996).

Optical methods using potentiometric dyes have been successfully utilized to measure activation patterns in thin slices of isolated tissue and on the surface of intact hearts (Efimov et al., 1994). Davidenko et al. (1992) and Pertsov et al. (1993) reported stable spiral waves of

activation in thin slices of sheep and dog epicardium. In three dimensions, though, these re-entrant patterns degenerate to polymorphic tachycardia (Gray et al., 1995) and fibrillation (Frazier et al., 1989).

At the cellular level, significant differences in the transient outward current (I_{to}) between the epicardial and endocardial myocytes have been suggested as a reason for the different action potential morphologies in these regions (see Antzelevitch et al. (1995) for a comprehensive review). In cardiomyocytes isolated from the rabbit, Fedida and Giles (1991) reported higher action potential plateau amplitude and I_{to} density in the epicardial cells compared to the endocardial cells. Hence regional differences in electrophysiology at the cellular level may manifest themselves as nonuniform phenomena at the organ level.

4.2. Electrical activation modeling

Following the tradition established by Hodgkin and Huxley (1952) for nerve cells, the large database of knowledge from voltage-clamp studies of cardiac cells has been incorporated into increasingly complex models for ionic currents (Beeler and Reuter, 1977; Noble, 1990). More recent models have also included information on intracellular ion fluxes (especially Ca^{2+}) determined using optical indicators and intracellular microelectrodes. The most sophisticated models of ventricular myocyte electrophysiology, like those developed by Rudy and colleagues (Luo and Rudy, 1991, 1994a; Zeng et al., 1995) include background and leakage currents, ionic currents through voltage-gated channels, pumps and exchangers, and intracellular Ca^{2+} transport between the cytoplasm, sarcoplasmic reticulum and intracellular buffers. These models can simulate many physiological phenomena, and they describe the underlying mechanisms of early- and delayed-afterdepolarizations and post-extrasystolic potentiation in the single myocyte (Luo and Rudy, 1994b). Similarly detailed models of the cardiac action potential have also been derived for atrial and Purkinje fiber cells (DiFrancesco and Noble, 1985).

In addition to ionic currents, the propagation of excitation and repolarization must be modeled. Given a suitable membrane model, other factors that affect propagation include: three-dimensional ventricular geometry and boundary conditions; anisotropic current diffusion with respect to fiber and sheet directions; discrete effects due to extracellular microstructure and the distribution of intercellular gap junctions and the specialized conducting tissues and cellular heterogeneity of the heart. The most general continuum models of cardiac electrical excitation fall within bidomain theory (Plonsey and Barr, 1984), which models the intracellular space and the interstitium as two anisotropic domains separated by the cell membrane. Bidomain models are essential for investigating many critical problems such as defibrillation which involve nonhomogeneous distributions of extracellular potential (Henriquez et al., 1996; Trayanova, 1996a,b; Pollard et al., 1997). If the anisotropy of cellular and interstitial conductivity are assumed to be the same (a monodomain formulation), then the problem may be expressed as a three-dimensional extension of the continuous reaction-diffusion equation from cable theory:

$$C_m \frac{\partial}{\partial t} V_m = \nabla \cdot \mathbf{D} \nabla V_m - I_{ion}$$

where C_m is the membrane capacity, V_m and I_{ion} are the transmembrane voltage and ionic current, respectively, **D** is the diffusion tensor and ∇ is the gradient operator. The diffusion tensor is anisotropic, simulating faster conduction in the fiber direction than transversely. With suitable choices for the nonlinear ionic current term (I_{ion}), which models the membrane kinetics, this continuum system admits spiral or (in three-dimensions) scroll-wave topologies corresponding to re-entrant activation (Winfree, 1991; Davidenko et al., 1995). The majority of continuum models have used the phenomenological FitzHugh–Nagumo (FHN) equations (Courtemanche et al., 1990; Panfilov and Keener, 1995). In this reaction-diffusion system, the ionic currents are approximated by a phenomenological relation with parameters chosen to approximate the basic excitation, recovery and refractoriness properties of the myocardium. Using three-dimensional FHN models, Winfree has shown that rotors are scroll waves organized about vortex filaments that can adopt complex topologies (Winfree, 1994). Nonuniform anisotropy due to the heterogeneous cardiac muscle fiber orientation has been studied in these continuous systems (Panfilov and Keener, 1993). Courtemanche and Winfree also reported propagation models using the Beeler–Reuter membrane model for the ionic currents (Courtemanche and Winfree, 1991). These simulations showed the spontaneous fractionation of re-entrant activation waves due to the effects of nonuniform diastolic interval on refractory period. Although continuum models ignore the discrete effects of cell-to-cell coupling on macroscopic propagation (Spach et al., 1981; Rudy and Quan, 1987), cellular discontinuities can be simulated by appropriate modifications to the diffusion model (Keener, 1991).

To model cardiac electrical propagation as a nonuniformly anisotropic continuum, Rogers and McCulloch developed a collocation-Galerkin FE method for modeling excitable media (Rogers, 1993; Rogers and McCulloch, 1994a). The FE formulation demonstrated significant improvements over finite difference methods in its spatial and temporal convergence (Courtemanche and Winfree, 1991; Rogers et al., 1997). To permit anisotropic propagation with respect to a fiber axis that varies spatially within a single finite element, the equations are transformed to a local orthonormal coordinate system with one axis that is always aligned with the fiber direction. The collocation method is used to assemble the partial differential equations into a system of ordinary differential equations (ODEs) that are satisfied exactly at collocation points in each finite element. The boundary conditions are handled using a Galerkin approach to overcome the limitations of collocation techniques over irregular boundaries (Frind and Pinder, 1979). The resulting system of ODEs is solved through time using an adaptive Runge–Kutta scheme. With a modification of FHN kinetics, these new methods were used to identify a mechanism for spiral wave drift and scroll wave breakup in tissue with nonuniform muscle fiber angles (Rogers and McCulloch, 1994b).

Besides continuum models, numerical simulations of cardiac electrical activity include cellular automata and resistively coupled network models. Cellular automata (Thakor and Eisenman, 1989; Bailie et al., 1990) are simple, flexible and computationally efficient, but their rule-based propagation and discrete membrane potential waveforms preclude an accurate representation of the electrotonic interactions between neighboring regions of myocardium. Resistively coupled network models have been used to simulate intercellular coupling more realistically (Lesh et al., 1989). They have been useful for investigating the effects of anisotropic extracellular coupling on membrane capacitance charging factors, safety

factors and propagation velocities. But accordingly, they are more complex and computationally expensive than cellular automata or continuum models. Resistive networks may be helpful for deriving new macroscopic models, but it is still impractical to extend them to the whole heart.

5. Development of a structural model

In this section we describe in detail the development of a new model of the rabbit ventricles, an important animal model of cardiac mechanics (Kang and Yin, 1996), electrophysiology (Gillis et al., 1996), mechanoenergetics (Watkins et al., 1996) and excitation–contraction coupling (Kentish et al., 1992; Bluhm and Lew, 1995). The computational procedures outlined here closely follow those developed by Nielsen et al. (1991), though we have chosen the rabbit because many of the most suitable experiments for validating three-dimensional models of this kind have been conducted in this species (Franz et al., 1992; Lew et al., 1994; Gray et al., 1995). An electrophysiological model of a 9-g rabbit heart will have about one thirtieth the number of degrees of freedom of a comparably converged model of the dog heart, since the space constant for conduction is similar for both species (about 1 mm) (Osaka et al., 1987; Knisley and Hill, 1995). Nonetheless, with appropriately timed extrastimuli, the rabbit model is still large enough to admit the complex re-entrant dynamics that can also be evoked in larger species (Allessie et al., 1989; Hill et al., 1990; Schalij et al., 1992).

5.1. Experimental preparation

New Zealand white rabbits (3.8–4.1 kg) were anesthetized with 50 mg/kg ketamine hydrochloride and 4 mg/kg xylazine hydrochloride and ventilated with oxygen and 1.5% halothane. A sternotomy was performed, the aorta clamped and 3 mg/kg heparin sodium injected into the left ventricle (LV). The heart was arrested in diastole using a hyperkalemic cardioplegic solution (29.5 mM KCl).

The heart was immediately excised, the pulmonary vessels removed and the chordae tendineae cut to prevent valve closure during fixation. The aorta was cannulated and the heart suspended in Ringers lactate solution, then perfused in the unloaded state with 10% buffered formalin phosphate at 80 mm Hg for 3–4 min. The heart was stored in 10% buffered formalin phosphate until sectioned.

5.2. Tissue processing

The right and left ventricular cavities were filled with a quick-setting dental rubber (polyvinylsiloxane). Two 25 gauge needles were inserted in orthogonal directions at the apex in the short-axis plane; the needles prevent the heart from moving relative to the surrounding rubber. The whole heart was placed in a custom-built rigid tube and plunger assembly. The open volume between the heart and tube was also filled with dental rubber. Three hemispherical notches (machined parallel to the tube axis on the inner surface) provide a 'tongue-in-groove' key that prevented the heart and surrounding rubber from rotating within

the tube. On the face of the tube are four crosshair fiducial markers (visible in each panel of Fig. 1) used for later registering the images of the short-axis slices.

After a setting time of 3–5 min, successive short-axis digital images (640 × 480 pixels, 0.13 mm/pixel) of the tissue, rubber and fiducial markers were acquired as 2–3 mm thick slices of the rubber and tissue were cut from the face of the tube (Fig. 1). From these images the geometric contours of the tissue–rubber interface were segmented and the geometric coordinates of the fiducial markers are recorded using standard image processing software (NIH Image). The last slice contained the LV apex and geometric minimum of the epicardium. These points were highlighted with small white dots of titanium dioxide and their geometric coordinates also recorded. With tissue slice thickness information, the geometric contours and fiducial markers constitute a three-dimensional geometric representation of the right and left ventricular epicardial and endocardial surfaces.

Myocardial fiber measurements are collected from blocks of tissue cut from the slices in a radial direction. Each block was mounted on a cryostage and serially sectioned in the plane tangent to the epicardium (shown schematically in Fig. 2a). Measurements of the local myocardial fiber angle relative to the slice plane were made at four central locations in images of unstained 20-μm sections from the epicardial tangent plane (Fig. 2b). Selected sections from a typical block are shown in Fig. 3. High magnification images of the sections showed an average sarcomere length of 2.06 ± 0.12 SD μm ($n = 133$), consistent with the intact myocardium in diastasis (Sonnenblick et al., 1967), suggesting there was minimal systematic dilation or shrinkage in this preparation.

5.3. Image registration and coordinate transformations

The heart and tube assembly had to be removed from the imaging apparatus to cut successive short-axis slices. Since the assembly could not be replaced exactly in the previous imaging position, a reference image was chosen and a translation–rotation transformation determined for each of the other images to register the fiducial markers. After applying these transformations to the contours of the tissue-rubber interface, the geometric coordinates of the cardiac surfaces were consistent with a global 'measurement' coordinate system (Fig. 4a).

To develop the mathematical model, it is convenient to define a 'model' coordinate system relative to features of the heart (Fig. 4b). Since no anatomical features have the same geometric position from one heart to the next, we chose to locate the x_1-axis of the model coordinate system on a line through the LV apex and the LV cavity centroid in the slice nearest the equator. The origin of the model coordinate system is located at the origin of the best-fit ellipsoid to the LV cavity contours; this best-fit ellipsoid also gives the focus position d (Eq. (1)). The x_2-axis of the model system was located at the bisection of the line from the right ventricular (RV) cavity corners in the same nearest-equatorial slice.

5.4. Surface and fiber fitting

Before fitting, the three-dimensional geometric coordinates were converted to prolate spheroidal coordinates, which enables the surface fits to be reduced to one dimension (Nielsen et al., 1991). The circumferential θ coordinate of the six nodes on the vertical RV boundary

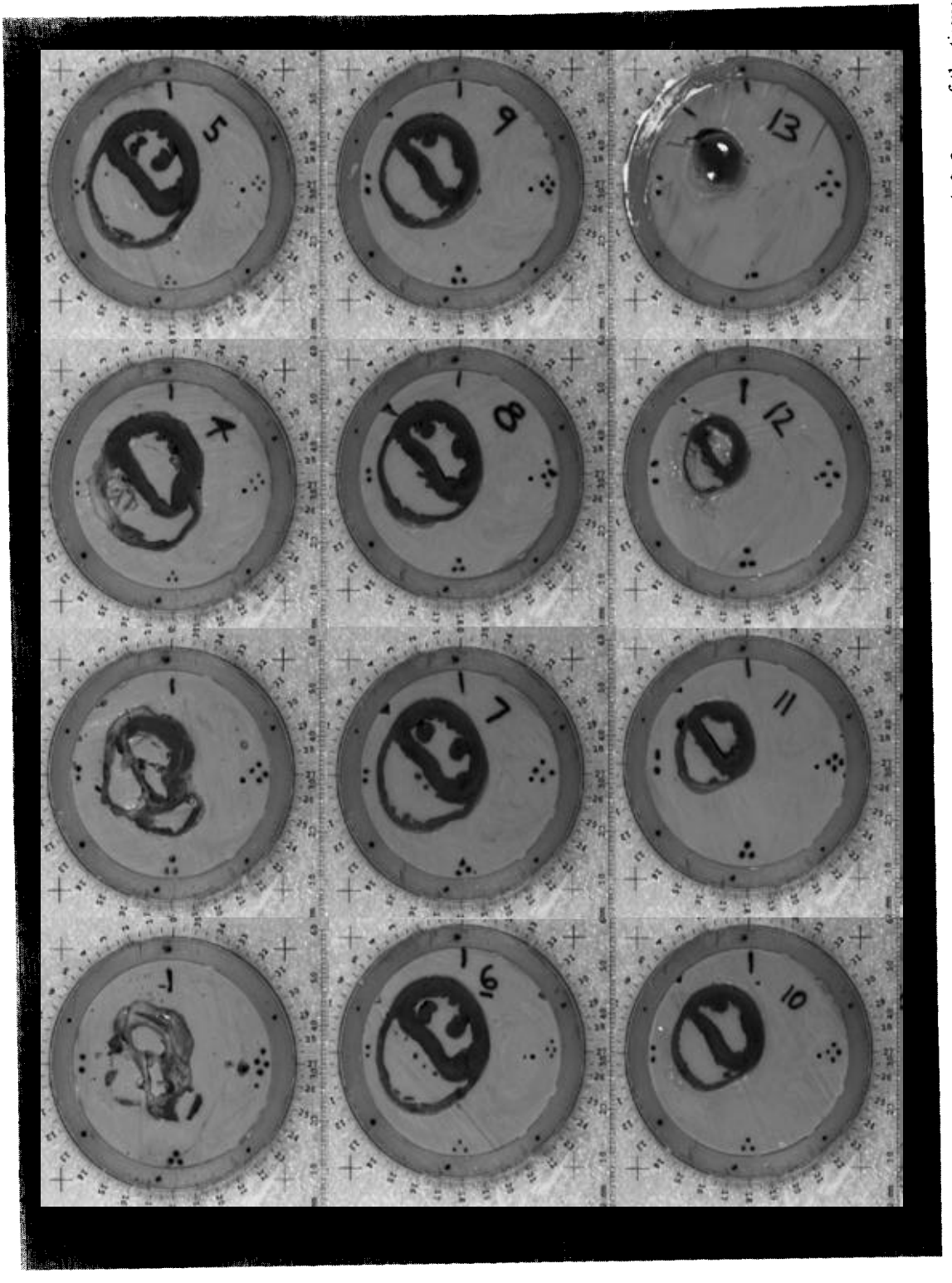

Fig. 1. Successive serial images of the short-axis slices of myocardium cast in dental rubber. After each image was captured, 2–3 mm of the tissue/rubber plug were pressed out of the tube and sliced off, exposing the myocardium and rubber for the next image. Successive images are shown in rows starting at the base (upper left) and ending at the apex (lower right).

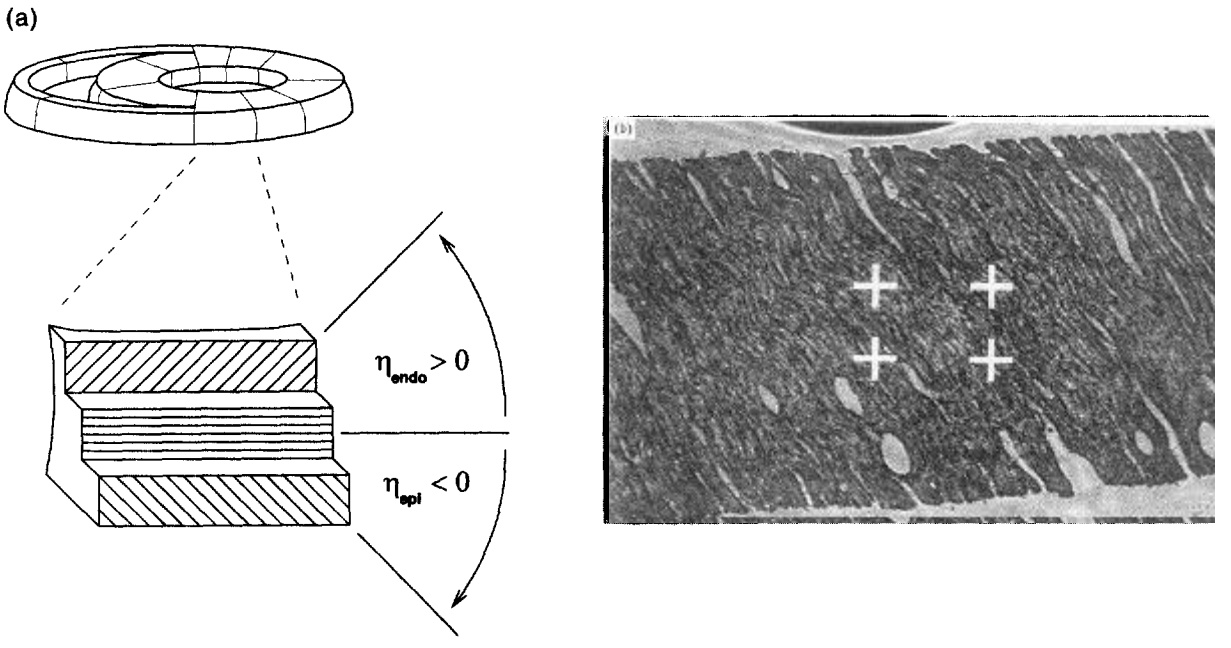

Fig. 2. (a) Schematic of a block cut from a tissue slice, showing the transmural variation in fiber angle η. (b) Micrograph (6.68×) of unstained cryosectioned tissue showing fiber orientations. White crosses indicate the typical locations of the four fiber angle measurements. Angles were measured with respect to the lower edge of the tissue. In the section shown the average measured fiber angle was −61°.

was fitted (6 DOF) to the extremal geometric coordinates in this region. The longitudinal μ coordinate of the 20 basal nodes was fitted (20 DOF) to the geometric contours of the first slice of myocardium. Finally, using the method of Nielsen and coworkers (Nielsen et al., 1991), the radial λ coordinate of the nodes defining the four two-dimensional finite element meshes (48 total elements), one each for the left ventricular endocardium, the epicardium and right ventricular free and septal walls, was simultaneously fitted (226 DOF) to the coordinates of the cardiac surfaces using a constrained linear least-squares method. The constraints imposed on the fit ensure derivative symmetry at the left ventricular apex and the epicardial geometric minimum and derivative equality at the right ventricular free and septal wall boundaries.

Owing to the sparsity of geometric coordinates in the apical (last) slice, the radial positions of the nodes at the LV apex and epicardial geometric minimum were not fitted; instead, these nodal variables were assigned the geometric coordinates of the titanium oxide dots at these locations. The remaining radial coordinates were fitted to 8,351 geometric coordinates, interpolated with bicubic Hermite basis functions (Hunter et al., 1988; Nielsen et al., 1991) to provide derivative continuity on the surfaces. To generate the single three-dimensional volumetric mesh from the four two-dimensional meshes, additional nodes were defined in the LV midwall and the two-dimensional surface elements were connected transmurally by defining nodal interconnections through the myocardial walls. The final three-dimensional mesh of 36 elements (552 total DOF) defines the geometry of the ventricular model and was used to fit the fiber angle measurements.

Fig. 3. Typical images (6.68×) of serial cryosections of unstained tissue from the inferior septum. Normalized transmural wall depth of the sections (from left to right, starting at upper left): 7, 15, 26, 36, 53, 64, 72, 86 and 99%. Total thickness of the block was 3.66 mm. Average measured fiber angle in the first section is −104°; in the last section this average is +43°.

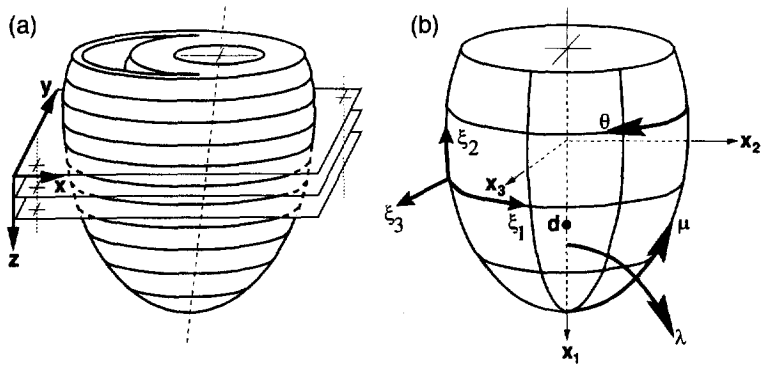

Fig. 4. Schematic diagrams of the 'measurement' and 'model' coordinate systems. (a) Locations of the individual slices are represented by planes, which are parallel to each other but not perpendicular to the long-axis of the LV cavity. (b) The rectangular Cartesian 'model' coordinate system (x_1, x_2, x_3) is collinear with the long-axis of the LV cavity. The prolate spheroidal coordinate system (λ, μ, θ) is convenient for modeling cardiac geometry. The curvilinear parametric coordinates (ξ_1, ξ_2, ξ_3), used in fitting and subsequent analysis, are the local finite element coordinates.

The geometric coordinates of the first and last serial tissue section of each block were mapped onto the geometric model to define the location of the measured fiber angles relative to the model. The measured fiber angles were then mapped to the appropriate transmural positions in the model and corrected for the difference between the plane of the tissue slices (to which the measured angles were referenced) and the curvilinear local finite element circumferential plane (the ξ_1–ξ_3 plane, to which the angles are referenced in the model). This correction is required because the plane of the tissue slices is not, in general, parallel to the ξ_1–ξ_3 plane in the three-dimensional elements. Redundant nodes at the RV boundary (like those used by Nielsen et al. (1991)) allow for the abrupt change in fiber angle in these regions. Fitted fiber angles at the nodes along the RV endocardial circumferential boundary were constrained to be equal to those at the corresponding nodes in the apical midwall, again owing to the sparsity of measurements in this region. The same constraint was applied to a single node at the RV endocardial boundary at the base. Over 14,300 local fiber angle measurements from 3,592 serial sections were fitted (184 degrees of freedom) using bilinear-cubic Hermite basis functions.

5.5. Results

The fitted three-dimensional finite element model of the ventricular geometry and fiber angles is shown in Fig. 5. The root mean squared errors (RMSE) of the geometric and fiber fits are summarized by region in Table 1. Over 22,500 measurements are represented by 736 degrees of freedom with a RMSE of $\pm$0.55 mm in the geometric surfaces and $\pm$19° in the fiber angles. A comparison of the measured fiber angles and the fitted transmural distributions is shown in Fig. 6. The fitted fiber distributions are in close agreement with the measured angles and the fitted distributions in the dog (Nielsen et al., 1991).

Gross anatomical information can be extracted from the model (Table 2). The volumes of the LV free wall, septum, RV free wall and apex are calculated from the three-dimensional

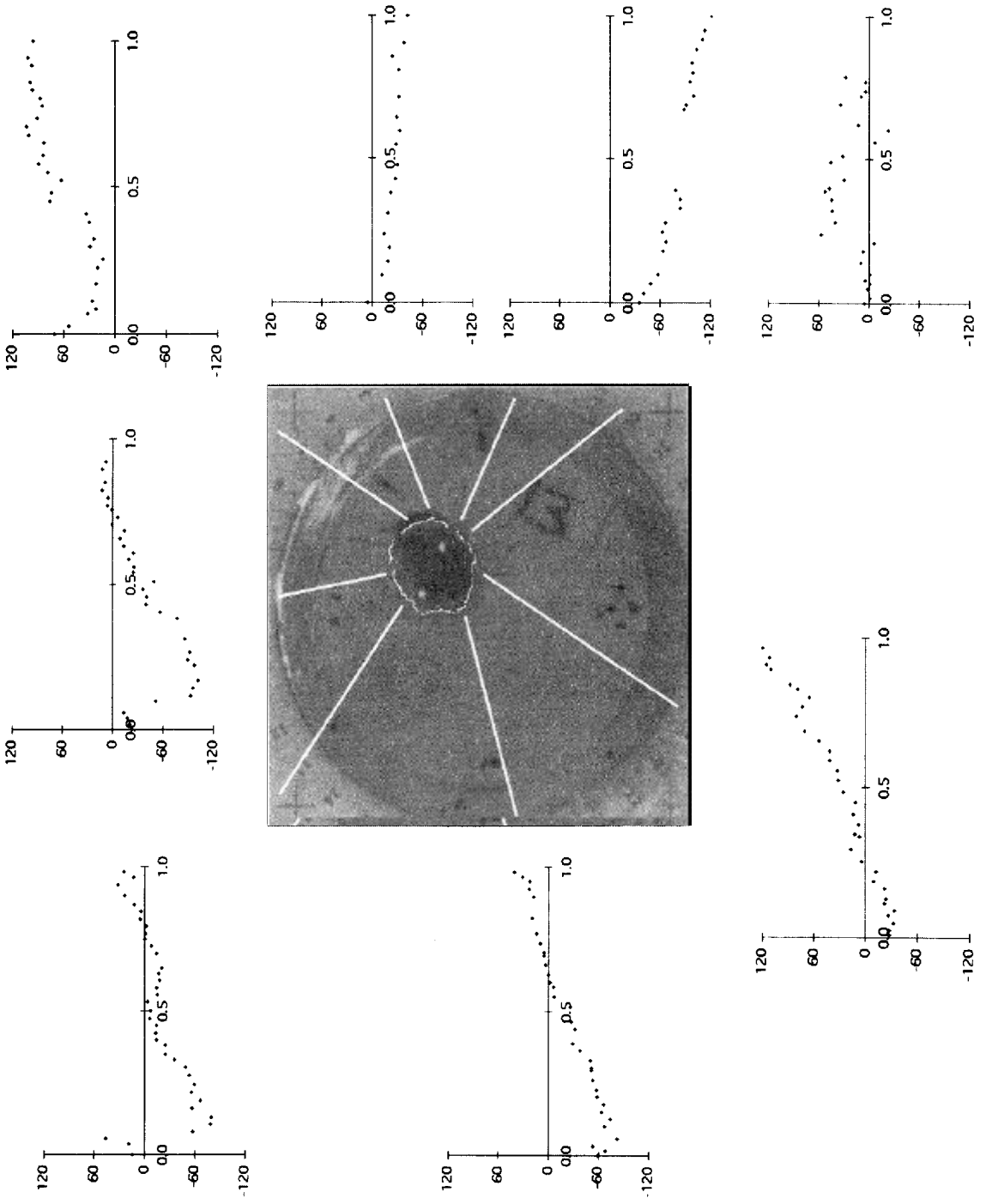

Fig. 7. Measured, uncorrected fiber angles from eight apical tissue blocks. The white contour outlines tissue-rubber boundary. White dots at lower right and upper left arc lowest points of the LV and RV cavities, respectively. White lines indicate direction of the transmural sectioning path which ended at the lower right dot. Plot axes are fiber angle (vertical scale: −120 to +120°) versus normalized wall depth (horizontal scale: 0.0 is epicardium, 1.0 is endocardium). Note the negative transmural gradient in the plots on the right.

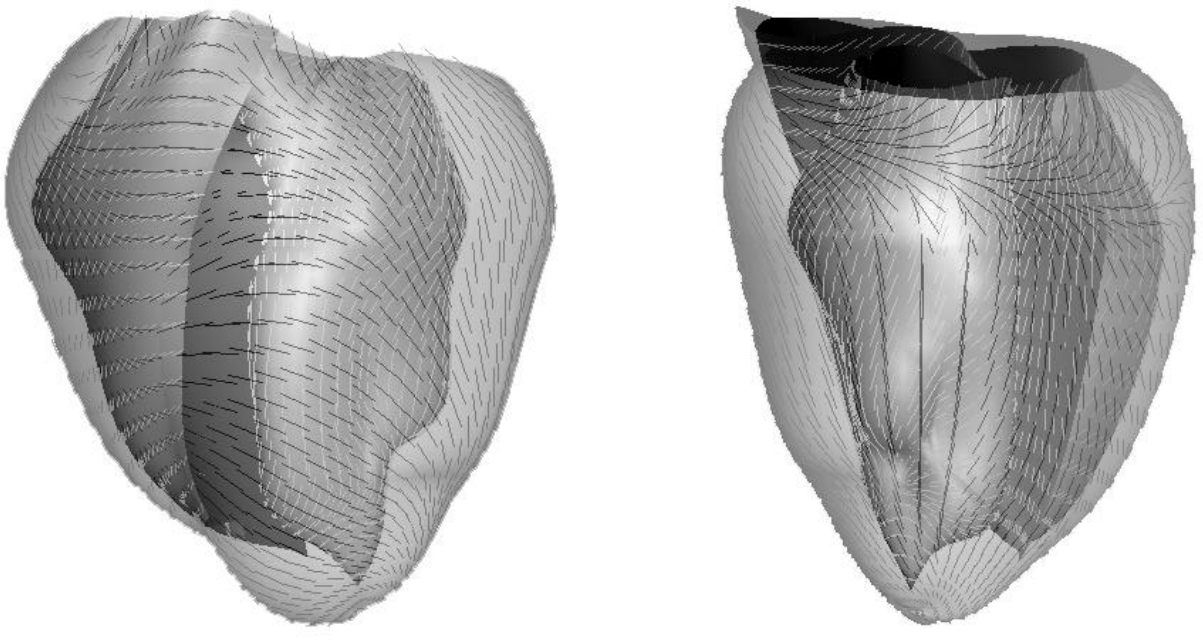

Fig. 5. Anterior (LEFT) and posterior lateral (RIGHT) views of the fitted three-dimensional finite element model showing interpolated fiber angles superposed on epicardial and endocardial surfaces.

element volumes representing those regions in the actual heart. The average thickness of the same elements was used to determine wall thickness. The RV and LV cavity volumes, 2.49 and 1.75 ml, imply the RV was probably distended while being filled with dental rubber. The transmural fiber distributions were the interpolated values along a line in the equatorial plane at the circumferential midpoint of each region, except the apex, where the angles are interpolated from the longitudinal midpoint of the apical elements in the lateral wall. The fitted fiber distribution errors are all below 20° except at the apex, where gradients of measured fiber angles were primarily monotonic, but demonstrated distinct transition from a positive transmural gradient to a negative gradient in the anterior region (Fig. 7). We attribute this sudden change shift in transmural fiber gradient direction to the transition of fibers from sub-epicardium to sub-endocardium where the imbrication angle of the fibers is greatest (Streeter, 1979), Using higher-order interpolation functions in the longitudinal direction, together with the a nodal imbrication angle parameter in the basal and apical regions should reduce the fitted fiber distribution errors.

The fitted geometric coordinate values and fiber angles are shown in Tables 3 and 4. The detailed model can be simplified by omitting the derivatives and interpolating only the fitted geometric value and fiber angle parameters using trilinear Lagrange basis functions. Although this approach increases the total RMSE of the geometric model to ± 1.10 mm and the fiber distribution RMSE to $\pm 24.1°$ (detailed by region in Table 5), for some applications the simplified computations may justify the reduced accuracy[1].

[1] Both the detailed and simplified models are available via the World-Wide Web at http://cmrg.ucsd.edu/

Table 1
Root mean squared errors (RMSE) in the fitted finite element geometry (552 DOF) and fiber distribution (184 DOF) models

Heart region	Geometry points	RMSE (mm)	Fibers # sections	RMSE (degrees)	No. of elements
LVFW	3200	0.35	1569	15.4	12
RVFW	3157	0.72	599	18.3	6
Septum	1514	0.47	852	11.9	6
Apex	480	0.61	572	31.1	12
overall	8351	0.55	3592	18.6	36

6. Future directions: coupled models of the heart

The electrical and mechanical function in the intact heart are based on complex cellular ionic mechanisms. While much is known about these mechanisms at the one-dimensional cellular level, relating how these mechanisms interact to affect the global behavior of the whole heart depends on the three-dimensional geometry and anisotropy of the intact myocardium.

The cardiac cycle is initiated by an electrical stimulus resulting in fiber shortening, causing contraction; known as excitation–contraction coupling, this process is typically considered to be 'one-way'. There is evidence, however, that a feedback pathway exists, whereby the electrical characteristics of myocardium are altered by the mechanical state of the tissue. This phenomena of mechanoelectric feedback may play a significant role in the regulation of normal electrical function and the genesis of arrhythmias (see Franz (1996, 1995) and Crozatier (1996) for comprehensive reviews).

The discovery of stretch-activated ion channels in myocardium (Sigurdson et al., 1987; Craelius et al., 1988) has led to speculation that these cellular structures are responsible for the mechanical sensitivity of electrical processes in the intact heart. Ruknudin and coworkers (Ruknudin et al., 1993) identified five distinct stretch-activated ion channels (SACs) in cardiac myocytes that are K^+ and cation selective. In isolated myocytes, increasing sarcomere length did not affect resting membrane potential or action potential amplitude but significantly decreased the action potential duration and the magnitude of the intracellular calcium transient (White et al., 1993). In the presence of extracellular Ca^{2+}, mechanical stimulation of chick embryo cardiomyocytes can cause waves of calcium-induced calcium release (Sigurdson et al., 1992) that are prevented by 20 mM gadolinium, a blocker of SACs (Yang and Sachs, 1989).

In isolated canine hearts, action potential amplitude and duration and the susceptibility to premature depolarizations are altered by ventricular dilatation (Hansen et al., 1990; Franz et al., 1992; Hansen, 1993; Zabel et al., 1996a). Gadolinium also reversibly suppresses stretch-induced arrhythmias in isolated canine hearts (Hansen et al., 1991; Stacy et al., 1992). Increases in left ventricular volume have been shown to decrease action potential (AP) duration and increase dispersion of repolarization in the isolated rabbit heart (Zabel et al., 1996b). In contrast, decreasing the load on contracting myofibers increases AP duration in strips of frog ventriculax myocardium (Lab, 1980). Patients undergoing balloon valvuloplasty for pulmonary stenosis showed a significant increase in AP duration and QT interval (Levine et al., 1988). Ischemia and sustained stretch increase dispersion of repolarization in the intact isolated rabbit (Kurz et al., 1993; Zabel et al., 1996b), which may produce a favorable environment for

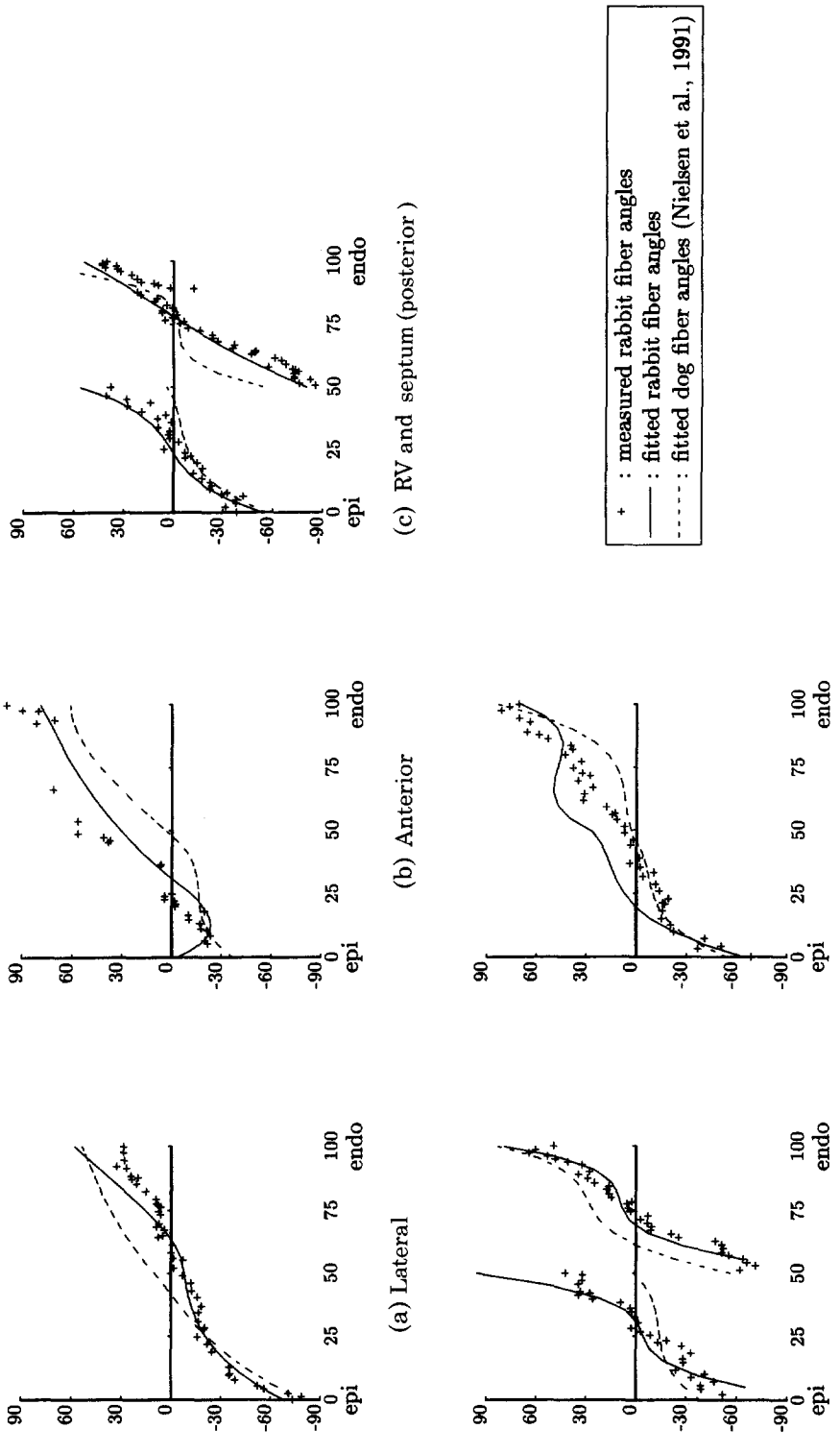

Fig. 6. Measured and fitted fiber angles for the rabbit (crosses and solid lines) and fitted fiber angles for the dog. Horizontal axes are normalized wall depth (%); vertical axes are fiber angle (degrees).

Table 2
Anatomical information from the finite element model

Heart region	Volume (ml)	Average wall thickness (mm)	Transmural fiber angle distribution (degrees)	
			epicardium	endocardium
LV free wall	3.42	4.98	−71.0	59.6
Septal wall	1.36	4.88	−45.1	51.5
RV free wall	1.35	1.69	−78.2	28.0
Apex	0.48	3.49	−29.6	69.3

reentry (Kuo et al., 1985). Additionally, using transient stretch pulses, Zabel et al. (1996a) reported stretch-induced depolarizations of varying magnitude and stretch-induced arrhythmias at different epicardial regions of the left ventricle of the isolated rabbit heart; they suggested the origin of the stretch-induced depolarization is not randomly located, but occurs at the location of highest stretch. Lekven et al. (1979) showed that step increases in end-diastolic left ventricular diameter reduced epicardial action potential amplitude by 14.7%, while endocardial action potential amplitude was reduced by 27.8%. This nonuniform transmural response to stretch may be associated with the significant transmural gradient of diastolic cross-fiber strain (Omens et al., 1991).

The existence of SACs, in light of the intact organ studies described above, suggest that SACs are at least in part responsible for the mechanically-induced changes observed in the electrical function of the heart. By adding SAC parameters to Noble's OxSoft HEART model, Sachs (1994) conducted one-dimensional simulations with results qualitatively similar to observations in experimental preparations of Purkinje fibers, ventricular cells and the whole organ. Bluhm (1995) recently modified the 'phase II' Luo–Rudy ionic model (Luo and Rudy, 1994a) to study the slow phase of the Fank–Starling response to a step change in myocyte length. The analysis suggested that transmembrane sodium ion fluxes may be strain dependent, but this result is yet to be verified.

Hence, there is substantial evidence for mechanoelectric as well as electromechanical coupling in the normal heart, but most detailed information lies at the single cell level. That these mechanosensitive properties affect cardiac impulse propagation in the whole heart seems clear but how they produce the interactions between electrical conduction and mechanical function in the intact heart is unknown because there are no three-dimensional models of cardiac electromechanical coupling or suitable experimental approaches for studying these interactions in the whole heart. There are only scant data on how two-dimensional and three-dimensional mechanics depend on two-dimensional or three-dimensional activation patterns (Waldman and Covell, 1987; Waldman et al., 1994; Delhaas et al., 1996) and essentially none on how multi-dimensional activation and recovery patterns depend on regional stress or strain. Yet without this information, there is little prospect for integrating the result of detailed cellular studies back to the level of the intact heart.

It is clear that coupled, multiscale models are required. The continuum framework supports a wide range of analyses appropriate to the intact myocardium by allowing cellular properties to be included in the constitutive laws and microstructural detail to be included in the

Table 3
Fitted prolate spheroidal geometric coordinates (λ, μ, θ) and fiber angles (η) in the LV wall and apex, excluding derivatives. Focus d = 13.29 mm. Coordinate values μ, θ and fiber angle η are in degrees; the λ coordinate is dimensionless. See text for discussion

Region	Epicardium				LV midwall				LV endocardium			
	μ	θ	λ	η	μ	θ	λ	η	μ	θ	λ	η
Base	118.81	50.751	0.85587	163.38	123.80	50.751	0.68504	5.9867	129.16	50.751	0.44017	−8.0727
	116.90	125.00	0.77879	53.824	121.51	125.00	0.62236	33.294	126.12	125.00	0.46593	100.37
	129.64	250.00	0.71123	−72.463	133.09	250.00	0.51355	32.546	136.54	250.00	0.31586	42.909
	124.41	283.16	1.0629	−43.435	125.80	282.79	0.98015	−4.2603	137.32	281.91	0.36250	78.118
Mid	90.00	70.898	0.84819	−37.142	90.00	70.898	0.73965	69.169	90.00	70.898	0.35657	63.359
	90.00	125.00	0.77315	−91.549	90.00	125.00	0.63522	−16.048	90.00	125.00	0.49729	75.354
	90.00	250.00	0.69948	−44.937	90.00	250.00	0.58290	−0.50420	90.00	250.00	0.46632	39.603
	90.00	307.74	0.92556	39.571	90.00	307.74	0.85618	−24.452	90.00	307.74	0.50333	118.50
	27.00	55.378	0.88807	−32.496	27.00	55.378	0.85321	3.6419	27.00	55.378	0.57724	34.932
	40.00	125.00	0.70523	−88.129	40.00	125.00	0.49725	34.972	40.00	125.00	0.28926	69.780
	40.00	250.00	0.64705	−37.802	40.00	250.00	0.48005	34.253	40.00	250.00	0.31305	123.66
	40.00	335.48	0.89627	−94.723	40.00	335.48	0.86512	41.523	40.00	335.48	0.60243	45.200
Apex	0.00	–	0.91900	6.8298	0.00	–	0.86950	8.3762	0.00	–	0.82000	45.147

Table 4
Fitted prolate spheroidal geometric coordinates (λ, μ, θ) and fiber angles (η) in the (a) RV and (b) septal walls, excluding derivatives. Focus d = 13.29 mm. Coordinate values μ, θ and fiber angle η are in degrees; the λ coordinate is dimensionless. See text for discussion

(a) Right ventricular free wall

Region	Epicardium				RV endocardium			
	μ	θ	λ	η	μ	θ	λ	η
Base	124.41	283.16	1.0629	−43.435	125.80	282.79	0.98015	−14.542
	121.42	301.81	1.1687	120.17	122.88	300.00	1.1474	−24.761
	121.96	343.23	1.0802	−149.31	122.82	343.23	0.96135	181.460
	118.81	50.751	0.85587	163.38	123.80	50.751	0.68504	−41.311
Mid	90.00	307.74	0.92556	39.571	90.00	307.74	0.85618	−45.051
	90.00	336.00	1.0315	−117.54	90.00	336.00	0.94621	97.764
	90.00	4.3166	1.1208	−71.218	90.00	4.3166	1.0505	15.674
	90.00	70.898	0.84819	−37.142	90.00	70.898	0.73965	97.036
	40.00	335.48	0.89627	−94.723	40.00	335.48	0.86512	41.523
	35.00	357.00	0.88674	−142.13	35.00	357.00	0.79233	7.0367
	31.00	20.429	0.88346	40.636	31.00	20.429	0.83939	−4.3418
	27.00	55.378	0.88807	−32.496	27.00	55.378	0.85321	3.6419

(b) Septal wall

Region	RV endocardium				LV endocardium			
	μ	θ	λ	η	μ	θ	λ	η
Base	125.80	282.79	0.98015	−4.2603	137.32	281.91	0.36250	78.118
	125.56	300.00	0.94373	22.499	130.45	319.23	0.72481	−63.278
	129.11	343.23	0.78889	−73.139	133.80	343.23	0.54247	−47.308
	123.80	50.751	0.68504	−30.118	129.16	50.751	0.44017	−8.0727
Mid	90.00	307.74	0.85618	−86.681	90.00	307.74	0.50333	118.50
	90.00	336.00	0.69423	−121.24	90.00	336.00	0.25560	81.181
	90.00	4.3166	0.47084	−31.668	90.00	4.3166	0.18885	46.254
	90.00	70.898	0.73965	−129.46	90.00	70.898	0.35657	63.359
	40.00	335.48	0.86512	−55.216	40.00	335.48	0.60243	45.200
	35.00	357.00	0.79233	−53.720	35.00	357.00	0.53948	55.272
	31.00	20.429	0.83939	−192.93	31.00	20.429	0.52467	−4.6942
	27.00	55.378	0.85321	−60.695	27.00	55.378	0.57724	34.932

Table 5
RMSE by region for the simplified model using trilinear Lagrange interpolation of the fitted coordinate values and fiber angles

	LVFW	RVFW	Septum	Apex	Overall
Geometry (mm)	0.80	0.75	1.27	1.29	1.10
Fiber (degrees)	20.5	28.5	17.8	34.2	24.1

geometric description of the whole heart. These models will be necessarily be simplified approximations since data are incomplete, especially on the effects of different multiaxial strain components (such as cross-fiber strain) and the biophysics of SACs. However, simplified models can provide a basis for studying the possibility of anisotropic coupling by investigating how stretch-dependent model parameters affect the agreement between the coupled FE models and experimental studies in the whole heart. Since no investigations have measured the relationship between the magnitude of strain and propagation, new experimental studies must be designed to obtain quantitative information on the tensor relationships between two-dimensional epicardial conduction, regional strains and stretch-dependent currents mediated by stretch-activated channels.

The mechanical and electrical problems are computationally large, although individually they can be solved on modern engineering workstations. A coupled electromechanical model of the whole heart will require high-performance computing. Fortunately, there is substantial scope for parallel implementations of these models that promise to make a wide range of new numerical experiments possible. Most previous high performance simulations of activation have used vector supercomputers (Courtemanche and Winfree, 1991; Rogers and McCulloch, 1994a), but there have also been some notable examples of models using massively parallel architectures (Kogan et al., 1991; Winslow et al., 1995). In cardiac mechanics, the best examples of high-performance analyses are the immersed boundary models of ventricular fluid flows by Peskin and McQueen (1992).

A wide variety of electromechanical and mechanoelectric models are possible. The major limitation is the lack of comprehensive experimental data on quantitative relationships, particularly on mechanoelectric feedback in two and three dimensions. Nevertheless, much is known, especially at the cellular level, and the FE model provides a foundation to extend these results to the level of the whole organ. While it is not yet practical to implement a fully comprehensive model that includes all known electromechanical interactions, individual models of specific interactions will be possible, for example: the effects of pacing site on strain distributions; the effects of stretch-dependent currents on three-dimensional action potential conduction; and the effects of excitation–contraction coupling mechanisms measured in isolated cells on the history-dependence of ventricular mechanics. These models promise to have diverse applications in cardiac physiology, analysis of pacemaker design and placement and cardiac tissue engineering and surgery techniques.

Acknowledgements

This work was supported by a National Science Foundation grant BES-9634974 and the National Biomedical Computation Resource (NIH grant, RR08065). We are grateful to Rish Pavelec and Babak Fazeli for excellent technical support, Dr. James Covell for use of his laboratory, Dr. Peter Hunter and Dr. Alistair Young for advice on mesh fitting, Walt Baxter and Dr. Kevin Costa for several enlightening technical discussions and undergraduate students Scott Moonly, Stephanie Pao and Jessica Wagenseil for their histological skills and perseverance.

References

Allessie, M.A., Schahj, M.J., Kirchhof, C.J., Boersma, L., Huybers, M., Hollen, J., 1989. Experimental electrophysiology and arrhythmogenicity. Anisotropy and ventricular tachycardia. Eur. Heart J. 10 Supplement E, 2–8.

Antzelevitch, C., Sicouri, S., Lukas, A., Nesterenko, V.V., Liu, D.-W., Di Diego, J.M., 1995. Regional differences in the electrophysiology of ventricular cells: Physiological and clinical implications. In: Zipes, D.P., Jalife, J. (Eds.), Cardiac Electrophysiology: From Cell to Bedside, 2nd ed. W.B. Saunders, Philadelphia, ch. 23, pp. 228–245.

Azhari, H., Weiss, J.L., Rogers, W.J., Sin, C.O., Zerhouni, E.A., Shapiro, E.P., 1993. Noninvasive quantification of principal strains in normal canine hearts using tagged MRI images in 3D. Am. J. Physiol. 264 (Heart Circ. Physiol. 33), H205–H216.

Bailie, A.H., Mitchell, R.H., Anderson, J.M., 1990. A computer model of re-entry in cardiac tissue. Comput. Biol. Med. 20 (1), 47–54.

Beeler, G.W., Reuter, H., 1977. Reconstruction of the action potential of ventricular myocardial fibres. J. Physiol. 268 (1), 177–210.

Bluhm, W.F., 1995. Length–history dependence of myocardial contraction. Ph.D. thesis, University of California, La Jolla, California.

Bluhm, W.F., Lew, W.Y.W., 1995. Sarcoplasmic reticulum in cardiac length-dependent activation in rabbits. Am. J. Physiol. 269 (Heart Circ. Physiol. 38), H965–H972.

Bovendeerd, P.H., Arts, T., Huyghe, J.M., van Campen, D.H., Reneman, R.S., 1992. Dependence of local left ventricular wall mechanics on myocardial fiber orientation: a model study. J. Biomech. 25 (10), 1129–1140.

Bovendeerd, P.H.M., Huyghe, J.M., Arts, T., van Campen, D.H., Reneman, R.S., 1994. Influence of endocardial–epicardial crossover of muscle fibers on left ventricular wall mechanics. J. Biomech. 27 (7), 941–951.

Brutsaert, D.L., 1987. Nonuniformity: A physiologic modulator of contraction and relaxation of the normal heart. J. Am. Coll. Cardiol. 9 (2), 341–348.

Cabo, C., Pertsov, A.M., Baxter, W.T., Davidenko, J.M., Gray, R.A., Jalife, J., 1994. Wave-front curvature as a cause of slow conduction and block in isolated cardiac muscle. Circ. Res. 75 (6), 1014–1028.

Cabo, C., Pertsov, A.M., Davidenko, J.M., Baxter, W.T., Gray, R.A., Jalife, J., 1996. Vortex shedding as a precursor of turbulent electrical activity in cardiac muscle. Biophys. J. 70 (3), 1105–1111.

Caulfield, J.B., Borg, T.K., 1979. The collagen network of the heart. Lab. Invest. 40 (3), 364–372.

Costa, K.D., 1996. The structural basis of three-dimensional ventricular mechanics. Ph.D. thesis, University of California, La Jolla, California.

Costa, K.D., Hunter, P.J., Rogers, J.M., Guccione, J.M., Waldman, L.K., McCulloch, A.D., 1996a. A three-dimensional finite element method for large elastic deformations of ventricular myocardium: I. Cylindrical and spherical polar coordinates. J. Biomech. Eng. 118 (4), 452–463.

Costa, K.D., Hunter, P.J., Rogers, J.M., Guccione, J.M., Waldman, L.K., McCulloch, A.D., 1996b. A three-dimensional finite element method for large elastic deformations of ventricular myocardium: II. Prolate spheroidal coordinates. J. Biomech. Eng. 118 (4), 464–472.

Courtemanche, M., Skaggs, W., Winfree, A.T., 1990. Stable three-dimensional action potential circulation in the FitzHugh–Nagumo model. Phys. D 41 (2), 173–182.

Courtemanche, M., Winfree, A.T., 1991. Re-entrant rotating waves in a Beeler–Reuter based model of two-dimensional cardiac electrical activity. Int. J. Bifurcation Chaos Appl. Sci. Eng. 1 (2), 431–444.

Craelius, W., Chen, V., El-Sherif, N., 1988. Stretch activated ion channels in ventricular myocytes. Biosci. Rep. 8 (5), 407–414.

Crozatier, B., 1996. Stretch-induced modifications of myocardial performance: from ventricular function to cellular and molecular mechanisms. Cardiovasc. Res. 32 (1), 25–37.

Davidenko, J.M., Pertsov, A.V., Salomonsz, R., Baxter, W.T., Jalife, J., 1992. Stationary and drifting spiral waves of excitation in isolated cardiac muscle. Nature 355 (6358), 349–351.

Davidenko, J.M., Salomonsz, R., Pertsov, A.M., Baxter, W.T., Jalife, J., 1995. Effects of pacing on stationary re-entrant activity: Theoretical and experimental study. Circ. Res. 77 (6), 1166–1179.

Delgado, C., Steinhaus, B., Delmar, M., Chivalvo, D.R., Jalife, J., 1990. Directional differences in excitability and margin of safety for propagation in sheep ventricular epicardial muscle. Circ. Res. 67 (1), 97–110.

Delhaas, T., Arts, T., Prinzen, F.W., Reneman, R.S., 1996. Regional electrical activation and mechanical function in the partially ischemic left ventricle of dogs. Am. J. Physiol. 271 (Heart Circ. Physiol. 40), H2411–H2420.

DiFrancesco, D., Noble, D., 1985. A model of cardiac electrical activity incorporating ionic pumps and concentration changes. Philos. Trans. R. Soc. London Ser. B: 307 (1133), 353–398.

Durrer, D., van Dam, R.T., Freud, G.E., Janse, M.J., Meijler, F.L., Arzbaecher, R.C., 1970. Total excitation of the isolated human heart. Circulation 41 (6), 899–912.

Efimov, I.R., Ermentrout, B., Huang, D.T., Salama, G., 1996. Activation and repolarization patterns are governed by different structural characteristics of ventricular myocardium: experimental study with voltage-sensitive dyes and numerical simulations. J. Cardiovasc. Electrophysiol. 7 (6), 512–530.

Efimov, I.R., Huang, D.T., Rendt, J.R.M., Salama, G., 1994. Optical mapping of repolarization and refractoriness from intact hearts. Circulation 90 (3), 1469–1480.

Fedida, D., Giles, W.R., 1991. Regional variations in action potentials and transient outward current in myocytes isolated from rabbit left ventricle. J. Physiol. 442, 191–209.

Franz, M.R., 1995. Stretch-activated arrhythmias. In: Zipes, D.P., Jalife, J. (Eds.), Cardiac Electrophysiology: From Cell to Bedside, 2nd ed. W.B. Saunders, Philadelphia, ch. 57, pp. 597–606.

Franz, M.R., 1996. Mechano-electrical feedback in ventricular myocardium. Cardiovasc. Res. 32 (1), 15–24.

Franz, M.R., Cima, R., Wang, D., Profitt, D., Kurz, R., 1992. Electrophysiological effects of myocardial stretch and mechanical determinants of stretch-activated arrhythmias. Circulation 86(3), 968–978 (published erratum appears in Circulation 86(5), 1663).

Frazier, D.W., Wolf, P.D., Wharton, J.M., Tang, A.S., Smith, W.M., Ideker, R.E., 1989. Stimulus induced critical point: mechanism for electrical initiation of reentry in normal canine myocardium. J. Clin. Invest. 83 (3), 1039–1052.

Frind, E.O., Pinder, G.F., 1979. A collocation finite element method for potential problems in irregular domains. Int. J. Numer. Methods Eng. 14 (5), 681–701.

Gillis, A.M., Kulisz, E., Mathison, H.J., 1996. Cardiac electrophysiological variables in blood-perfused and buffer–perfused, isolated, working rabbit heart. Am. J. Physiol. 271 (Heart Circ. Physiol. 40), H784–H789.

Gray, R.A., Jalife, J., Panfilov, A.V., Baxter, W.T., Cabo, C., Davidenko, J.M., Pertsov, A.M., 1995. Nonstationary vortexlike reentrant activity as a mechanism of polymorphic ventricular tachycardia in the isolated rabbit heart. Circulation 91 (9), 2454–2469.

Greenbaum, R.A., Ho, S.Y., Gibson, D.G., Becker, A.E., Anderson, R.H., 1981. Left ventricular fibre architecture in man. Br. Heart J. 45 (3), 248–263.

Guccione, J.M., Costa, K.D., McCulloch, A.D., 1995. Finite element stress analysis of left ventricular mechanics in the beating dog heart. J. Biomech. 28 (10), 1167–1177.

Guccione, J.M., McCulloch, A.D., Waldman, L.K., 1991. Passive material properties of intact ventricular myocardium determined from a cylindrical model. J. Biomech. Eng. 113 (1), 42–55.

Hansen, D.E., 1993. Mechanoelectrical feedback effects of altering preload, afterload, and ventricular shortening. Am. J. Physiol. 264 (Heart Circ. Physiol. 33), H423–H432.

Hansen, D.E., Borganelli, M., Stacy, G.P., Jr., Taylor, L.K., 1991. Dose-dependent inhibition of stretch-induced arrhythmias by gadolinium in isolated canine ventricles. Evidence for a unique mode of antiarrhythmic action. Circ. Res. 69 (3), 820–831.

Hansen, D.E., Craig, C.S., Hondeghem, L.M., 1990. Stretch-induced arrhythmias in the isolated canine ventricle. Evidence for the importance of mechanoelectrical feedback. Circulation 81 (3), 1094–1105.

Henriquez, C.S., Muzikant, A.L., Smoak, C.K., 1996. Anisotropy, fiber curvature, and bath loading effects on activation in thin and thick cardiac tissue preparations: simulations in a three-dimensional bidomain model. J. Cardiovasc. Electrophysiol. 7 (5), 424–444.

Hill, B.C., Hunt, A.J., Courtney, K.R., 1990. Reentrant tachycardia in a thin layer of ventricular subepicardium: effects of D-sotalol and lidocaine. J. Cardiovasc. Pharmacol. 16 (6), 871–880.

Hodgkin, A.L., Huxley, A.F., 1952. A quantitative description of membrane current and its application to conduction and excitation in nerve. J. Physiol. 117, 500–544.

Hort, W., 1960. Makroskopische und mikrometrische untersuchungen am myokard verschieden stark gefüllter linker kammern. Virch. Arch. Pathol. Anat. Physiol. 333, 523–564.

Huisman, R.M., Elzinga, G., Westerhof, N., Sipkema, P., 1980. Measurement of left ventricular wall stress. Cardiovasc. Res. 14 (3), 142–153.

Humphrey, J.D., Yin, F.C.P., 1988. Biaxial mechanical behavior of excised epicardium. J. Biomech. Eng. 110(4), 349–351 (published erratum appears in J. Biomech. Eng. 1989, 111(3), 227).

Hunter, P.J., McCulloch, A.D., Nielsen, P.M.F., Smaill, B.H., 1988. A finite element model of passive ventricular mechanics. In: Spilker, R.L., Simon, B.R. (Eds.), Computational Methods in Bioengineering, vol. 9. American Society of Mechanical Engineers, New York, NY, pp. 387–397.

Hunter, P.J., Smaill, B.H., 1988. The analysis of cardiac function: a continuum approach. Prog. Biophys. Mol. Biol. 52 (2), 101–164.

Kang, T., Yin, F.C.P., 1996. The need to account for residual strains and composite nature of heart wall in mechanical analyses. Am. J. Physiol. 271 (Heart Circ. Physiol. 40), H947–H961.

Keener, J.P., 1991. Wave propagation in myocardium. In: Glass, L., Hunter, R., McCulloch, A. (Eds.), Theory of Heart: Biomechanics, Biophysics and Nonlinear Dynamics of Cardiac Function. Springer-Verlag, New York, ch. 17, pp. 405–436.

Kentish, J.C., Davey, R., Largen, P., 1992. Isoprenaline reverses the slow force responses to a length change in isolated rabbit papillary muscle. Pfluegers Arch. Eur. J. Physiol. 421 (5), 519–521.

Knisley, S.B., Hill, B.C., 1995. Effects of bipolar point and line stimulation in anisotropic rabbit epicardium: assessment of the critical radius of curvature for longitudinal block. IEEE Trans. Biomed. Eng. 42 (10), 957–966.

Kogan, B.Y., Karplus, W.J., Billett, B.S., Pang, A.T., Karagueuzian, H.S., Khan, S.S., 1991. The simplified FitzHugh–Nagumo model with action potential duration restitution: effects on 2D wave propagation. Phys. D 50 (3), 327–340.

Kuo, C.S., Reddy, C.P., Munakata, K., Surawicz, B., 1985. Mechanism of ventricular arrhythmias caused by increased dispersion of repolarization. Eur. Heart J. 6 (Suppl. D), 63–70.

Kurz, R.W., Ren, X.-L., Franz, M.R., 1994. Dispersion and delay of electrical restitution in the globally ischaemic heart. Eur. Heart J. 15 (4), 547–554.

Kurz, R.W., Xiao-Lin, R., Franz, M.R., 1993. Increased dispersion of ventricular repolarization and ventricular tachyarrhythmias in the globally ischaemic rabbit heart. Eur. Heart J. 14 (11), 1561–1571.

Lab, M.J., 1980. Transient depolarisation and action potential alterations following mechanical changes in isolated myocardium. Cardiovasc. Res. 14 (11), 624–637.

Lee, M.C., Fung, Y.C., Shabetai, R., LeWinter, M.M., 1987. Biaxial mechanical properties of human pericardium and canine comparisons. Am. J. Physiol. 253 (Heart Circ. Physiol. 22), H75–H82.

LeGrice, I.J., Hunter, P.J., Smaill, B.H., 1997. Laminar structure of the heart: a mathematical model. Am. J. Physiol. 272 (Heart Circ. Physiol. 41), H2466–H2476.

LeGrice, I.J., Smaill, B.H., Chai, L.Z., Edgar, S.G., Gavin, J.B., Hunter, P.J., 1995. Laminar structure of the heart: ventricular myocyte arrangement and connective tissue architecture in the dog. Am. J. Physiol. 269 (Heart Circ. Physiol. 38), H571–H582.

Lekven, J., Chatterjee, K., Tyberg, J.V., Parmley, W.W., 1979. Reduction in ventricular endocardial and epicardial potentials during acute increments in left ventricular dimensions. Am. Heart J. 98 (2), 200–206.

Lesh, M.D., Pring, M., Spear, J.F., 1989. Cellular uncoupling can unmask dispersion of action potential duration in ventricular myocardium. A computer modeling study. Circ. Res. 65 (5), 1426–1440.

Levine, J.H., Guarnieri, T., Kadish, A.H., White, R.L., Calkins, H., Kan, J.S., 1988. Changes in myocardial repolarization in patients undergoing balloon valvuloplasty for congenital pulmonary stenosis: evidence for contraction–excitation feedback in humans. Circulation 77 (1), 70–77.

Lew, W.Y., Nishikawa, Y., Su, H., 1994. Cardiac myocyte function and left ventricular strains after brief ischemia and reperfusion in rabbits. Circulation 90 (4), 1942–1950.

Lew, W.Y.W., 1987. Influence of ischemic zone size on nonischemic area function in the canine left ventricle. Am. J. Physiol. (Heart Circ. Physiol. 21) 252, H990–H997.

Luo, C.-H., Rudy, Y., 1991. A model of the ventricular cardiac action potential: depolarization, repolarization, and their interaction. Circ. Res. 68 (6), 1501–1526.

Luo, C.-H., Rudy, Y., 1994a. A dynamic model of the cardiac ventricular action potential. I. Simulations of ionic currents and concentration changes. Circ. Res. 74 (6), 1071–1096.

Luo, C.-H., Rudy, Y., 1994b. A dynamic model of the cardiac ventricular action potential. II. Afterdepolarizations, triggered activity, and potentiation. Circ. Res. 74 (6), 1097–1113.

McCulloch, A.D., 1995. Cardiac biomechanics. In: Bronzino, J.D. (Ed.), Biomedical Engineering Handbook, CRC Press: IEEE Press, Boca Raton, ch. 31, pp. 418–439.

McCulloch, A.D., Guccione, J.M., Waldman, L.K., Rogers, J., 1993. Large-scale finite element analysis of the beating heart. In: Pilkington, T.C., Loftis, B., Thompson, J.F., Woo, S.L.-Y., Palmer, T.C., Budinger, T.F. (Eds.), High Performance Computing in Biomedical Research. CRC Press, Boca Raton, FL, pp. 27–49.

McCulloch, A.D., Omens, J.H., 1991. Factors affecting the regional mechanics of the diastolic heart. In: Glass, L., Hunter, R., McCulloch, A. (Eds.), Theory of Heart: Biomechanics, Biophysics and Nonlinear Dynamics of Cardiac Function. Springer-Verlag, New York, ch. 5, pp. 87–119.

McCulloch, A.D., Smaill, B.H., Hunter, P.J., 1989. Regional left ventricular epicardial deformation in the passive dog heart. Circ. Res. 64 (4), 721–733.

Moore, C.G., O'Dell, W.G., McVeigh, E.R., Zerhouni, E.A., 1992. Calculation of three-dimensional left ventricular strains from biplanar tagged MR images. J. Magnetic Resonance Imaging 2 (2), 165–175.

Nielsen, P.M.F., LeGrice, I.J., Smaill, B.H., Hunter, P.J., 1991. Mathematical model of geometry and fibrous structure of the heart. Am. J. Physiol. 260 (Heart Circ. Physiol. 29), H1365–H1378.

Noble, D., 1990. Ionic mechanisms in normal cardiac activity. In: Zipes, D.P., Jalife, J. (Eds.), Cardiac Electrophysiology: From Cell to Bedside. W.B. Saunders, Philadelphia, ch. 19, pp. 163–171.

Novak, V.R., Yin, F.C.R., Humphrey, J.D., 1994. Regional mechanical properties of passive myocardium. J. Biomech. 27 (4), 403–412.

Omens, J.H., Covell, J.W., 1991. Transmural distribution of myocardial tissue growth induced by volume-overload hypertrophy in the dog. Circulation 84 (3), 1235–1245.

Omens, J.H., Farr, D.D., McCulloch, A.D., Waldman, L.K., 1996. Comparison of two techniques for measuring two-dimensional strain in rat left ventricles. Am. J. Physiol. 271 (Heart Circ. Physiol. 40), H1256–H1261.

Omens, J.H., MacKenna, D.A., McCulloch, A.D., 1993. Measurement of strain and analysis of stress in resting rat left ventricular myocardium. J. Biomech. 26 (6), 665–676.

Omens, J.H., May, K.D., McCulloch, A.D., 1991. Transmural distribution of three-dimensional strain in the isolated arrested canine left ventricle. Am. J. Physiol. 261 (Heart Circ. Physiol. 30), H918–H928.

Osaka, T., Kodama, L., Tsuboi, N., Toyama, J., Yamada, K., 1987. Effects of activation sequence and anisotropic cellular geometry on the repolarization phase of action potential of dog ventricular muscles. Circulation 76 (1), 226–236.

Panfilov, A.V., Keener, J.P., 1993. Generation of reentry in anisotropic myocardium. J. Cardiovasc. Electrophysiol. 4 (4), 412–421.

Panfilov, A.V., Keener, J.P., 1995. Re-entry in an anatomical model of the heart. Chaos Solitons Fractals 5 (3/4), 681–689.

Pearlman, E.S., Weber, K.T., Janicki, J.S., Pietra, G.G., Fishman, A.P., 1982. Muscle fiber orientation and connective tissue content in the hypertrophied human heart. Lab. Invest. 46 (2), 158–164.

Pertsov, A.M., Davidenko, J.M., Salomonsz, R., Baxter, W.T., Jalife, J., 1993. Spiral waves of excitation underlie reentrant activity in isolated cardiac muscle. Circ. Res. 72 (3), 631–650.

Peskin, C.S., McQueen, D.M., 1992. Cardiac fluid dynamics. Crit. Rev. Biomed. Eng. 20 (5–6), 451–459.

Pinto, J.G., Fung, Y.C., 1973. Mechanical properties of the heart muscle in the passive state. J. Biomech. 6 (6), 597–616.

Plonsey, R., Barr, R.C., 1984. Current flow patterns in two-dimensional anisotropic bisyncytia with normal and extreme conductivities. Biophys. J. 45 (3), 557–571.

Pollard, A.E., Spitzer, K.W., Burgess, M.J., 1997. Contributions of the specialized conduction system to the activation sequence in the canine pulmonary conus. Am. J. Physiol. 273 (Heart Circ. Physiol. 42), H446–H463.

Province, R.A., Fishler, M.G., Thakor, N.V., 1993. Effects of defibrillation shock energy and timing on 3D computer model of heart. Ann. Biomed. Eng. 21 (1), 19–31.

Robb, J.S., Robb, R.C., 1942. The normal heart: Anatomy and physiology of the structural units. Am. Heart J. 23, 455–467.

Robinson, T.F., Cohen-Gould, L., Factor, S.M., 1983. Skeletal framework of mammalian heart muscle. Arrangement of inter- and pericellular connective tissue structures. Lab. Invest. 49 (4), 482–498.

Robinson, T.F., Geraci, M.A., Sonnenblick, E.H., Factor, S.M., 1988. Coiled perimysial fibers of papillary muscle in rat heart: morphology, distribution, and changes in configuration. Circ. Res. 63 (3), 577–592.

Rogers, J.M., 1993. Finite element modeling of cardiac activation dynamics. Ph.D. thesis, University of California, La Jolla, California.

Rogers, J.M., Courtemenche, M.S., McCulloch, A.D., 1997. Finite element methods for modelling impulse propagation in the heart. In: Panfilov, A.V., Holden, A.V. (Eds.), Computational Biology of the Heart. J. Wiley and Sons, West Sussex, England, ch. 7, pp. 217–234.

Rogers, J.M., McCulloch, A.D., 1994a. A collocation-Galerkin finite element model of cardiac action potential propagation. IEEE Trans. Biomed. Eng. 41 (8), 743–757.

Rogers, J.M., McCulloch, A.D., 1994b. Nonuniform muscle fiber orientation causes spiral wave drift in a finite element model of cardiac action potential propagation. J. Cardiovasc. Electrophysiol. 5 (6), 496–509.

Ross, M.A., Streeter, D.D., Jr., 1975. Nonuniform subendocardial fiber orientation in the normal macaque left ventricle. Eur. J. Cardiol. 3 (3), 229–247.

Rudy, Y., Quan, W., 1987. A model study of the effects of the discrete cellular structure on electrical propagation in cardiac tissue. Circ. Res. 61 (6), 815–823.

Ruknudin, A., Sachs, F., Bustamante, J.O., 1993. Stretch-activated ion channels in tissue-cultured chick heart. Am. J. Physiol. 264 (Heart Circ. Physiol. 33), H960–H972.

Sachs, F., 1994. Modeling mechanical–electrical transduction in the heart. In: Mow, V.C., Guilak, F., Hochmuth, R.M., Tran-Son-Tay, R. (Eds.), Cell Mechanics and Cellular Engineering. Springer-Verlag, New York, ch. 18, pp. 308–328.

Saffitz, J.E., Kanter, H.L., Green, K.G., Tolley, T.K., Beyer, E.C., 1994. Tissue-specific determinants of anisotropic conduction velocity in canine atrial and ventricular myocardium. Circ. Res. 74 (6), 1065–1070.

Schalij, M.J., Lammers, W.J.E.P., Rensma, P.L., Allessie, M.A., 1992. Anisotropic conduction and reentry in perfused epicardium of rabbit left ventricle. Am. J. Physiol. 263 (Heart Circ. Physiol. 32), H1466–H1478.

Sigurdson, W., Ruknudin, A., Sachs, F., 1992. Calcium imaging of mechanically induced fluxes in tissue-cultured chick heart: role of stretch-activated ion channels. Am. J. Physiol. 262 (Heart Circ. Physiol. 31), H1110–H1115.

Sigurdson, W.J., Morris, C.E., Brezden, B.L., Gardner, D.R., 1987. Stretch activation of a K^+ channel in molluscan heart cells. J. Exp. Biol. 127, 191–209.

Smaill, B. H., Hunter, P. J., 1991. Structure and function of the diastolic heart. In Glass, L., Hunter, R., McCulloch, A. (Eds.), Theory of Heart: Biomechanics, Biophysics and Nonlinear Dynamics of Cardiac Function. Springer-Verlag, New York, ch. 1, pp. 1–29.

Sonnenblick, E.H., Ross, J., Jr., Covell, J.W., Spotnitz, H.M., Spiro, D., 1967. The ultrastructure of the heart in systole and diastole. Changes in sarcomere length. Circ. Res. 21 (4), 423–431.

Spach, M.S., Miller III, W. T, Geselowitz, D.B., Barr, R.C., Kootsey, J.M., Johnson, E.A., 1981. The discontinuous nature of propagation in normal canine cardiac muscle: evidence for recurrent discontinuities of intracellular resistance that affect the membrane currents. Circ. Res. 48 (1), 39–54.

Stacy, G.P., Jr., Jobe, R.L., Taylor, L.K., Hansen, D.E., 1992. Stretch-induced depolarizations as a trigger of arrhythmias in isolated canine left ventricles. Am. J. Physiol. 263 (Heart Circ. Physiol. 32), H613–H621.

Streeter, D.D., Jr., 1979. Gross morphology and fiber geometry of the heart. In: Berne, R.M. (Ed.), Handbook of Physiology, Section 2: The Cardiovascular System, vol. 1. American Physiological Society, Bethesda, Maryland, ch. 4, pp. 61–112.

Streeter, D.D., Jr., Bassett, D.L., 1966. An engineering analysis of myocardial fiber orientation in pig's left ventricle in systole. Anat. Rec. 155 (4), 503–512.

Streeter, D.D., Jr., Hanna, W.T., 1973a. Engineering mechanics for successive states in canine left ventricular myocardium: I. Cavity and wall geometry. Circ. Res. 33, 639–655.

Streeter, D.D., Jr., Hanna, W.T., 1973b. Engineering mechanics for successive states in canine left ventricular myocardium: II. Fiber angle and sarcomere length. Circ. Res. 33, 656–664.

Streeter, D.D., Jr., Powers, W.E., Ross, M.A., Torrent-Guasp, F., 1978. Three-dimensional fiber orientation in the mammalian left ventricular wall. In: Baan, J., Noordergraaf, A., Raines, J. (Eds.), Cardiovascular System Dynamics. MIT Press, Cambridge, MA, pp. 73–84.

Streeter, D.D., Jr., Spotnitz, H.M., Patel, D.P., Ross, J., Jr., Sonnenblick, E.H., 1969. Fiber orientation in the canine left ventricle during diastole and systole. Circ. Res. 24 (3), 339–347.

Taber, L.A., 1991. On a nonlinear theory for muscle shells: Part II. Application to the beating left ventricle. J. Biomech. Eng. 113 (1), 63–71.

ter Keurs, H.E., Rijnsburger, W.H., van Heuningen, R., Nagelsmit, M.J., 1980. Tension development and sarcomere length in rat cardiac trabeculae: Evidence of length-dependent activation. Circ. Res. 46 (5), 703–714.

Thakor, N.V., Eisenman, L.N., 1989. Three-dimensional computer model of the heart: fibrillation induced by extrastimulation. Comput. Biomed. Res. 22 (6), 532–545.

Trayanova, N., 1996a. Discrete versus syncytial tissue behavior in a model of cardiac stimulation. I: Mathematical formulation. IEEE Trans. Biomed. Eng. 43 (12), 1129–1140.

Trayanova, N., 1996b. Discrete versus syncytial tissue behavior in a model of cardiac stimulation. II: Results of simulation. IEEE Trans. Biomed. Eng. 43 (12), 1141–1150.

Van Leuven, S.L., Waldman, L.K., McCulloch, A.D., Covell, J.W., 1994. Gradients of epicardial strain across the perfusion boundary during acute myocardial ischemia. Am. J. Physiol. 267 (Heart Circ. Physiol. 36), H2348–H2362.

Villarreal, F.J., Lew, W.Y., Waldman, L.K., Covell, J.W., 1991. Transmural myocardial deformation in the ischemic canine left ventricle. Circ. Res. 68 (2), 368–381.

Villarreal, F.J., Waldman, L.K., Lew, W.Y., 1988. Technique for measuring regional two-dimensional finite strains in canine left ventricle. Circ. Res. 62 (4), 711–721.

Waldman, L.K., Allen, J.J., McCulloch, A.D., 1994. Shear strain gradient during ventricular pacing. FASEB J. 8, A592 Abstract.

Waldman, L.K., Covell, J.W., 1987. Effects of ventricular pacing on finite deformation in canine left ventricles. Am. J. Physiol. 252 (Heart Circ. Physiol. 21), H1023–H1030.

Waldman, L.M., Fung, Y.C., Covell, J.W., 1985. Transmural myocardial deformation in the canine left ventricle: normal in vivo three-dimensional finite strains. Circ. Res. 57 (1), 152–163.

Waldman, L.K., Nosan, D., Villarreal, F., Covell, J.W., 1988. Relation between transmural deformation and local myofiber direction in canine left ventricle. Circ. Res. 63 (3), 550–562.

Watkins, M.W., Higashiyama, A., Chen, Z., LeWinter, M.M., 1996. Rapid shortening during relaxation increases activation and improves systolic performance. Circulation 94 (6), 1475–1482.

Weber, K.T., 1989. Cardiac interstitium in health and disease: the fibrillar collagen network. J. Am. Coll. Cardiol. 13 (7), 1637–1652.

White, E., Le Guennec, J.-Y., Nigretto, J.M., Gannier, F., Argibay, J.A., Garnier, D., 1993. The effects of increasing cell length on auxotonic contractions; membrane potential and intracellular calcium transients in single guinea-pig ventricular myocytes. Exp. Physiol. 78 (1), 65–78.

Winfree, A.T., 1991. Varieties of spiral wave behavior: an experimentalist's approach to the theory of excitable media. Chaos 1 (3), 303–334.

Winfree, A.T., 1994. Persistent tangled vortex rings in generic excitable media. Nature 371 (6494), 233–236.

Winslow, R.L., Cai, D., Varghese, A., Lai, Y.-C., 1995. Generation and propagation of normal and abnormal pacemaker activity in network models of cardiac sinus node and atrium. Chaos Solitons Fractals 5 (3–4), 491–512.

Yang, X.-C., Sachs, F., 1989. Block of stretch-activated ion channels in *Xenopus* oocytes by gadolinium and calcium ions. Science 243, 1068–1071 4894 Part 1.

Yin, F.C.P., Strumpf, R.M., Chew, P.H., Zeger, S.L., 1987. Quantification of the mechanical properties of noncontracting canine myocardium under simultaneous biaxial loading. J. Biomech. 20 (6), 577–589.

Young, A.A., Axel, L., 1992. Three-dimensional motion and deformation of the heart wall: estimation with spatial modulation of magnetization, a model-based approach. Radiology 185 (1), 241–247.

Young, A.A., Kramer, C.M., Ferrari, V.A., Axel, L., Reichek, N., 1994. Three-dimensional left ventricular deformation in hypertrophic cardiomyopathy. Circulation 90 (2), 854–867.

Zabel, M., Koller, B.S., Sachs, F., Franz, M.R., 1996a. Stretch-induced voltage changes in the isolated beating heart: importance of the timing of stretch and implications for stretch-activated ion channels. Cardiovasc. Res. 32 (1), 120–130.

Zabel, M., Portnoy, S., Franz, M.R., 1996b. Effect of sustained load on dispersion of ventricular repolarization and conduction time in the isolated intact rabbit heart. J. Cardiovasc. Electrophysiol. 7 (1), 9–16.

Zeng, J., Laurita, K.R., Rosenbaum, D.S., Rudy, Y., 1995. Two components of the delayed rectifier K^+ current in ventricular myocytes of the guinea pig type: theoretical formulation and their role in repolarization. Circ. Res. 77 (1), 140–152.